

## Nonlinear Compton scattering of polarized photons in plane-wave backgrounds

B. King<sup>\*</sup> and S. Tang<sup>†</sup>

*Centre for Mathematical Sciences, University of Plymouth, Plymouth PL4 8AA, United Kingdom*



(Received 20 March 2020; accepted 17 July 2020; published 13 August 2020)

We investigate the phenomenology of nonlinear Compton scattering of polarized photons by unpolarized electrons in plane-wave backgrounds. The energy and angular spectra of polarized photons are calculated for linearly and circularly polarized pulses, monochromatic fields and constant crossed field backgrounds. When the field intensity is in the weakly nonlinear regime, photons in different polarization states are predicted to possess very different energies and angular distributions. We explain this difference by calculating the spectrum for nonlinear Thomson scattering in a linearly polarized monochromatic background and projecting the electron's trajectory onto the different polarization directions. Finally, we calculate a scenario for multi-GeV electrons and, by considering the energy and angular-resolved photon polarization purity, find one can achieve a GeV-photon beam with polarization purities of over 90%.

DOI: [10.1103/PhysRevA.102.022809](https://doi.org/10.1103/PhysRevA.102.022809)

### I. INTRODUCTION

The process in which an electron collides with a laser pulse and absorbs more than a single laser photon before radiating is referred to as nonlinear Compton scattering (NLC):  $e \rightarrow e + \gamma$ . It has been studied theoretically in a constant crossed background [1], in a monochromatic plane wave [1–4], and in a finite pulse [5–9] and has been adapted to numerical Monte Carlo simulations [10–14]. Experimentally, up to the fourth harmonic has been observed in the E144 experiment [15], which collided a high-energy electron of 46.6 GeV with an intense laser pulse [16]. Evidence of the quantum effect of recoil in radiation reaction has recently been seen in laser-plasma experiments [17,18], and experimental campaigns in E320 at FACET-II [19] and in LUXE at DESY [20] plan to measure the transition of NLC to the nonperturbative regime.

There has been recent attention given to the description of electron and photon polarization in NLC. Using a non-precessing polarization basis [21], one can calculate the rate of polarization flip in single NLC events, which have been added to laser-plasma simulation codes [22]. It is necessary to introduce some asymmetry in the background field to prevent the spin-polarizing effect of the laser pulse from averaging out to zero, and various schemes such as counterpropagating pulses [23] or using an elliptically polarized beam [24] have been suggested to achieve higher spin-polarization purities. Using a simulation approach based on the locally constant field approximation (LCFA) [25–30] in the quantum-dominated radiation-reaction regime [31], it was recently suggested [32] that, by using high-energy *spin-polarized* electron beams colliding with an intense laser pulse, and an energy cut to the emitted photons, a highly polarized photon beam could

be achieved. At the same time as the current article was in preparation, Wistisen and Di Piazza [33] performed a QED calculation valid for arbitrary pulse length and spin-polarized electrons in a circularly polarized background, and they concluded that the deterioration in photon polarization purity that accompanies an increasing nonlinearity parameter can be compensated for by also using an angular cut.

A further importance of polarized single (dressed) vertex processes is their occurrence in higher-order processes. It has been shown several times [34–38] that, to correctly factorize the “two-step” trident process of NLC followed by nonlinear Breit-Wheeler pair creation, observed in the E144 experiment [39,40], one is required to consider the transverse polarization of the intermediate photon (whereas the “one-step” process involves all polarization states of the photon [41,42]). Analogously, in double NLC, it is the polarization of the intermediate electron that must be calculated for a correct factorization [21,43,44], and this “gluing” approach has recently been extended to QED cascades [45] (where a chain of dressed-vertex processes such as NLC and pair creation can occur [10,46–51]). Therefore it is of use to have expressions for polarized processes in a range of backgrounds, which also can be employed in higher-vertex calculations.

In the current paper, we focus on the polarization of the emitted photons in NLC and focus on the high-energy, intermediate intensity regime that is planned to be probed in E320 [19] and LUXE [20]. Being able to prepare high-energy photon beams with a high degree of polarization purity is advantageous for phenomenological studies. For example, it has been suggested that combining polarized high-energy photons with currently available laser facilities would allow the first measurement of real photon-photon scattering, either directly [52–55] or via the Kramer-Kronig relation that links the process to polarized Breit-Wheeler pair creation [56,57]. A general framework for incorporating polarized NLC to numerical simulations was derived in Ref. [11] and applied to study electromagnetic cascades in rotating electric fields.

<sup>\*</sup>b.king@plymouth.ac.uk

<sup>†</sup>suo.tang@plymouth.ac.uk

We derive photon-polarized NLC from unpolarized electrons in a pulsed plane-wave background and show that the energy and angular spectra of the emitted photons depend sensitively on their polarization states. Therefore, by using angular and energy cuts, one can achieve a significantly high degree of polarization. We find that the angular distribution of the photons in different polarization states are qualitatively different, exhibiting typical patterns of the different orders of multipole radiation. By deriving photon-polarized NLC in circularly and linearly polarized monochromatic backgrounds and comparing with a classical analysis of the electron trajectory, we find an explanation for the familiar multipole structures in the angular spectrum that can be traced to the projection of the electron's motion on the photon polarization directions.

The paper is organized as follows. Section II gives an overview of the finite-pulse derivation and defines important quantities that are used throughout the paper. In Sec. III, we outline the derivations for the production of linearly polarized photons in linearly polarized backgrounds: a pulsed field, a monochromatic field, and a constant crossed field, and then in Sec. IV, we proceed with the production of circularly polarized photons in circularly polarized backgrounds: a pulsed field, a monochromatic field, and a constant crossed field. In Sec. V, we display numerical results that show the significant discrepancy in the polarized photon energy spectrum and angular distribution by the QED result compared with the LCFA. In Sec. VI, we outline a classical calculation of the equivalent number of photons in the radiated field and demonstrate how, by decomposing the classical trajectory along the photon polarization directions, we recover the leading-order behavior of the QED result. In Sec. VII, we conclude.

## II. SCATTERING IN PULSE BACKGROUND

All the electromagnetic backgrounds we consider are of a transverse plane-wave nature with a reduced vector potential  $a(\phi) = eA(\phi)$ , for positron charge  $e$  and vector potential  $A$ , and  $\phi = \varkappa \cdot x$  is the external-field phase with wave vector  $\varkappa = \omega_0(1, 0, 0, 1)$  satisfying  $\varkappa^2 = 0$ ,  $\varkappa \cdot a = 0$ , and  $\omega_0$  is the field frequency. The scattering-matrix element for NLC is then

$$S_{fi} = -ie \int d^4x \bar{\psi}_q \not{\varepsilon}^* \psi_p \frac{e^{ik \cdot x}}{\sqrt{2V k^0}}, \quad (1)$$

where  $p$  and  $q$  are the incoming and outgoing electron momenta, respectively;  $k$  and  $\varepsilon$  are the scattered photon momentum and polarization, respectively, satisfying  $k \cdot \varepsilon = 0$ , and we recap the Volkov state

$$\psi_p = \left[ 1 + \frac{\not{\varepsilon} \not{a}(\phi)}{2 \varkappa \cdot p} \right] \frac{u_p}{\sqrt{2p^0 V}} e^{-ip \cdot x - i \int^\phi \frac{2p \cdot a(\varphi) - a^2(\varphi)}{2 \varkappa \cdot p} d\varphi}.$$

We wish to express the photon polarization in terms of the eigenstates of the polarization operator in the background field, which ensures photon polarization will not change after the emission. (The probability for photon-photon scattering [58] is very small, so that deviations in experiment from the plane-wave background are not expected to appreciably impact our assumption that the photon polarization remains constant after emission.) In linear background fields with

polarization  $\varepsilon_1 = (0, 1, 0, 0)$  [or  $\varepsilon_2 = (0, 0, 1, 0)$ ], the eigenpolarization can be expressed in terms of the orthogonal basis [59]:

$$\begin{aligned} \varepsilon_1 &= \varepsilon_1 - \frac{k \cdot \varepsilon_1}{k \cdot \varkappa} \varkappa, & \varepsilon_2 &= \varepsilon_2 - \frac{k \cdot \varepsilon_2}{k \cdot \varkappa} \varkappa, \\ e_\pm &= \pm k + \frac{1}{2k \cdot \varkappa} \varkappa, \end{aligned} \quad (2)$$

which satisfies the normalization:  $\varepsilon_1^2 = \varepsilon_2^2 = e_\pm^2 = -e_\mp^2 = -1$ , and up to a sign, the photon transverse polarization vectors are related to the invariants

$$\varepsilon_1 \sim \frac{k \cdot F}{\sqrt{-(k \cdot F)^2}}, \quad \varepsilon_2 \sim \frac{k \cdot \tilde{F}}{\sqrt{-(k \cdot \tilde{F})^2}},$$

where  $F$  is the Faraday field tensor and  $\tilde{F}$  its dual. However, in circular background fields with polarization  $(\varepsilon_1 \pm i\varepsilon_2)/\sqrt{2}$ , the eigenbases  $\varepsilon_{1,2}$  are replaced with

$$\varepsilon_{1,2} \rightarrow \varepsilon_\pm = \frac{1}{\sqrt{2}}(\varepsilon_1 \pm i\varepsilon_2).$$

Whilst we use a polarization basis related to the photon for its propagation through the background field, one should bear in mind that any measurement of the photon's polarization will necessarily involve a polarization basis specified by a *detector* (see, e.g., Sec. 65 of Ref. [60]). We are interested in the polarization of GeV photons, for which the process of pair polarimetry has been suggested as a method of measurement [54], which relies upon the Bethe-Heitler process of photon decay to an electron-positron pair in a Coulomb field.

We then calculate the probability  $P_j$  for NLC of a photon with polarization  $\varepsilon_j$  to be

$$P_j = V^2 \int \langle |\mathbf{S}_{fi}(\varepsilon_j)|^2 \rangle_{\text{spin}} \frac{d^3q d^3k}{(2\pi)^6}, \quad (3)$$

where  $\langle \cdot \rangle_{\text{spin}}$  refers to averaging over initial spins and summing over final spins of the electron,  $j = 1$  and  $2$  in the linear background field and  $j = +$  and  $-$  in the circular field. Expanding the photon polarization in the basis Eq. (2), only the photon's transverse polarization states ( $\varepsilon_1$  and  $\varepsilon_2$  in linear backgrounds,  $\varepsilon_+$  and  $\varepsilon_-$  in circular backgrounds) will survive, allowing us to write the total probability  $P$  as a sum of the probability of scattering into each of these polarization states  $P = P_1 + P_2$  ( $P = P_+ + P_-$ ) for linear (circular) background fields. Since the only nontrivial dependency on  $x$  is in the dependency on  $\varkappa \cdot x$ , one acquires a momentum-conserving  $\delta$  function in three coordinates, and we choose to integrate out the scattered electron momentum  $q$ . Eventually we arrive at the intermediate stage:

$$\begin{aligned} P_j &= \frac{\alpha}{(2\pi)^2} \frac{1}{\eta_p^2} \int_0^1 \frac{s}{t} ds \int d^2r^\perp \int d\phi d\phi' \\ &\times [\mathbf{T}(\varepsilon_j) e^{ic(\phi - \phi') - i \int_{\phi'}^\phi \frac{2p \cdot a(\varphi) - a^2(\varphi)}{2 \varkappa \cdot p} d\varphi}], \end{aligned} \quad (4)$$

where  $\alpha = e^2/4\pi$  is the fine-structure constant,  $\eta_p = \varkappa \cdot p/m^2$ ,  $s = \varkappa \cdot k/\varkappa \cdot p$  is the light-front momentum fraction of the scattered photon,  $t = 1 - s$ , and  $c = (k^+ + q^+ - p^+)/2\varkappa^0$ . We use light-front coordinates:  $x^\pm = x^0 \pm x^3$ ,  $x^\perp = (x^1, x^2)$ , and  $r^\perp = k^\perp/sm$  is the normalized photon momentum in the plane perpendicular to

the laser propagation direction, and it relates directly to the outgoing angle of the scattered photon:

$$r^\perp = \frac{m\eta_p}{\omega_0} \frac{\sin\theta}{1 + \cos\theta} (\cos\psi, \sin\psi), \quad (5)$$

where  $\theta$  is the polar angle measured from a head-on collision of the photon with the laser pulse and  $\psi$  is the azimuthal angle. The dependence of the emission probability  $\mathbf{P}_j$  on the photon polarization state  $\epsilon_j$  is included in

$$\mathsf{T}(\epsilon_j) = \bar{E}_q(\phi) \epsilon_j^* E_p(\phi) \bar{E}_p(\phi') \epsilon_j E_q(\phi'),$$

and we use the shorthand

$$E_p(\phi) = \left[ 1 + \frac{\kappa\phi(\phi)}{2\kappa \cdot p} \right] \frac{u_p}{\sqrt{2p^0}}.$$

### III. LINEARLY POLARIZED PHOTON

A linearly polarized background field has linearly polarized photon eigenstates. Here, we consider a laser background of the following form:

$$a(\phi) = m\xi g(\phi) \sin(\phi) \epsilon_1, \quad (6)$$

which has polarization  $\epsilon_1$ , intensity parameter  $\xi$ , and pulse envelope  $g(\phi)$ .

The derivation is very similar to that of the well-known unpolarized case [1,2]. Performing the calculation for  $\mathsf{T}(\epsilon_j)$ , we arrive at the linearly polarized photon-momentum spectrum:

$$\begin{aligned} \frac{d^3\mathbf{P}_j}{dsd^2r^\perp} &= \frac{\alpha}{(2\pi)^2} \frac{1}{\eta_p^2} \frac{s}{t} \int d\phi \int d\phi' e^{i(\phi-\phi') \langle \frac{k \cdot \pi_p}{\kappa \cdot q} \rangle} \\ &\times \left[ \Pi(\phi) \cdot \epsilon_j \Pi(\phi') \cdot \epsilon_j + \Delta \frac{s^2}{8t} \right], \end{aligned} \quad (7)$$

where we define the instantaneous classical electron momentum in a plane wave,

$$\pi_p(\phi) = p - a(\phi) + \kappa \frac{2p \cdot a(\phi) - a^2(\phi)}{2\kappa \cdot p},$$

and use the following shorthand:  $\Delta = [a(\phi) - a(\phi')]^2/m^2$ ,  $\Pi(\phi) = \pi_p(\phi)/m - k/ms$ . The window average of  $f$  is denoted by  $\langle f \rangle = (\phi - \phi')^{-1} \int_{\phi'}^{\phi} f(\varphi) d\varphi$ . Equation 7 contains a (divergent) contribution from a pure phase term, which persists outside the laser pulse and therefore must be regularized. Since we are interested in angular distributions, we cannot use the standard “ $i\epsilon$ ” prescription [61,62], but instead must regularize in the way introduced in Ref. [5] and recently further developed in Ref. [30]. This then leads to inserting regulation factors  $R(\phi)$  [ $R(\phi')$ ],

$$R(\phi) = 1 - \frac{k \cdot \pi_p(\phi)}{k \cdot p}, \quad (8)$$

wherever necessary in Eq. (7) to ensure the integrand is zero outside the pulse, which means  $\Pi(\phi) \rightarrow \Pi_{\text{reg.}}(\phi)$ :

$$\Pi_{\text{reg.}}(\phi) = -\ell R(\phi) - a(\phi)/m, \quad (9)$$

where  $\ell$  is the normalized shifted momentum:

$$\ell = \frac{k}{sm} - \frac{p}{m}. \quad (10)$$

So far this derivation has been quite general; we now specify it in a standard way to short pulses by defining an average  $\varphi = (\phi + \phi')/2$  and interference phase  $\vartheta = \phi - \phi'$  [29,63,64]. Integrating over the transverse momentum  $k^\perp$  [65], we arrive at the photon-polarized light-front-momentum spectrum:  $\mathbf{P}_{1,2} = (\mathbf{P} \pm \Delta\mathbf{P})/2$ , where  $\mathbf{P} = \mathbf{P}_1 + \mathbf{P}_2$  is the total unpolarized probability and  $\Delta\mathbf{P} = \mathbf{P}_1 - \mathbf{P}_2$  is the change in probability due to scattering into a particular polarization state:

$$\frac{d\mathbf{P}}{ds} = \frac{\alpha}{\pi\eta_p} \int d\varphi \left( \int_0^\infty \frac{d\vartheta}{\vartheta} \mathcal{K} - \frac{\pi}{2} \right), \quad (11a)$$

$$\frac{d\Delta\mathbf{P}}{ds} = \frac{\alpha}{\pi\eta_p} \int d\varphi \int_0^\infty \frac{d\vartheta}{\vartheta} (\alpha_1 - \alpha_2) \sin\left(\frac{s\vartheta\mu}{2\eta_p t}\right), \quad (11b)$$

where

$$\mathcal{K} = \left( 1 - \Delta \frac{1+t^2}{4t} \right) \sin\left(\frac{s\vartheta\mu}{2\eta_p t}\right),$$

the Kibble mass  $\mu = \mu(\varphi, \vartheta) = 1 - \langle a^2 \rangle/m^2 + \langle a \rangle^2/m^2$ , and  $\alpha_j = [\langle a \cdot \epsilon_j \rangle - a(\phi) \cdot \epsilon_j][\langle a \cdot \epsilon_j \rangle - a(\phi') \cdot \epsilon_j]/m^2$ . One significant difference in the standard derivation of NLC in a pulse is that, when one considers polarized electrons or photons, a term arises of the following form:

$$\int \frac{d\vartheta}{\vartheta^2} e^{if(\vartheta)}, \quad (12)$$

in addition to the usual terms with preexponent integrands of the form  $1/\vartheta$ . The regularization of this term proceeds in the same way as for the  $1/\vartheta$  term (i.e., one can write  $1/\vartheta^2 = -d(1/\vartheta)/d\vartheta$ , integrate by parts, and use the Sokhotsky-Plemelj theorem on the remaining  $1/\vartheta$  term). (The regularization of this integral has also been dealt with in Ref. [61].)

#### A. Photon-polarized NLC LCFA

The LCFA can be acquired from Eq. (7) by performing a Taylor series in the interference phase. To make the connection, let us specify the *field* to be  $a'(\varphi) = m\xi(\varphi) \epsilon_1$ , where  $\xi(\varphi)$  includes the pulse amplitude and the wave form. Then making the following substitutions,

$$\Delta \rightarrow -\vartheta^2 \xi^2(\varphi),$$

$$\vartheta \left\langle \frac{k \cdot \pi_p}{\kappa \cdot q} \right\rangle \rightarrow \frac{k \cdot \pi_p(\varphi)}{t\eta_p} \vartheta + \frac{1}{24} \frac{s\xi^2(\varphi)}{t\eta_p} \vartheta^3,$$

$$\Pi(\phi) \cdot \epsilon_j \Pi(\phi') \cdot \epsilon_j \rightarrow [\Pi(\varphi) \cdot \epsilon_j]^2 - \vartheta^2 \frac{\xi^2(\varphi)}{4} \delta_{1,j},$$

in Eq. (7), one can simply perform the integral over  $\vartheta$  to acquire the polarized photon triple differential spectrum:

$$\frac{d^3\mathbf{P}_j}{dsd^2r^\perp} = \frac{\alpha}{\pi\eta_p} \int d\varphi \text{Ai}(y) \left[ [\Pi(\varphi) \cdot \epsilon_j]^2 z + \delta_{1,j} y + \frac{s^2}{2t} y \right], \quad (13)$$

where

$$y = \frac{2k \cdot \pi_p(\varphi)}{s} z, \quad z = \left( \frac{s}{\chi_p t} \right)^{2/3},$$

and  $\chi_p = \chi_p(\varphi) = |\xi(\varphi)|\eta_p$ . We note that this angular-resolved LCFA result depends not only on the local electric

field  $\xi(\varphi)$  but also on the local vector potential  $a(\varphi)$  included in  $\pi(\varphi)$ . Integrating over transverse momenta  $k^\perp$ , the light-front momentum spectrum becomes

$$\frac{dP}{ds} = -\frac{\alpha}{\eta_p} \int d\varphi \left[ \text{Ai}_1(z) + \frac{1+t^2}{t} \frac{1}{z} \text{Ai}'(z) \right], \quad (14a)$$

$$\frac{d\Delta P}{ds} = \frac{\alpha}{\eta_p} \int d\varphi \frac{1}{z} \text{Ai}'(z), \quad (14b)$$

which is just an integration over the pulse shape of the NLC result in a constant crossed field [21].

### B. Linearly polarized monochromatic background

Beginning with Eq. (7), we derive photon-polarized NLC for a linearly polarized monochromatic background [corresponding to  $g(\phi) = 1$  in Eq. (6)]. The main complication introduced by linear polarization of the background is that  $a^2$  is not constant. This means that one is faced with a squared sinusoidal function in the exponent and preexponent. These can be handled straightforwardly by a Fourier decomposition. To this end, let us define the functions  $\Gamma_{l,n}$  via

$$\cos^h \phi e^{i(-\zeta_l \sin \phi + \beta \sin 2\phi)} = \sum_{n=-\infty}^{\infty} \Gamma_{h,n} e^{-in\phi}, \quad (15)$$

where

$$\zeta_l = \frac{s\xi}{t\eta_p} \ell \cdot \varepsilon_1, \quad \beta = \frac{s\xi^2}{8t\eta_p}. \quad (16)$$

We then find that  $\Gamma_{h,n} = \sum_{m=-\infty}^{\infty} J_m(\beta) F_{h,m,n}(\zeta_l)$ , with

$$\begin{aligned} F_{0,m,n} &= J_{2m+n}(\zeta_l), \\ F_{1,m,n} &= \frac{1}{2} [J_{2m+n+1}(\zeta_l) + J_{2m+n-1}(\zeta_l)], \\ F_{2,m,n} &= \frac{1}{4} [J_{2m+n+2}(\zeta_l) + 2J_{2m+n}(\zeta_l) + J_{2m+n-2}(\zeta_l)]. \end{aligned}$$

where  $J_n(\zeta_l)$  is the Bessel function. Unlike for the pulsed background case, there is no need to introduce an explicit regularization (being infinite in extent, there is no place where the monochromatic background disappears). Finally, we find  $P_j = \sum_{n=-\infty}^{\infty} P_{j,n}$ , where

$$\begin{aligned} P_{j,n} &= \frac{\alpha N_\phi}{\eta_p^2} \int_0^1 ds \int d^2 r^\perp \frac{s}{t} \delta(c + 2\beta - n) \\ &\times \left[ (\ell \cdot \varepsilon_j \Gamma_{0,n} - \delta_{1j} \xi \Gamma_{1,n})^2 \right. \\ &\left. - (\Gamma_{2,n} \Gamma_{0,n} - \Gamma_{1,n}^2) \frac{s^2 \xi^2}{4t} \right], \quad (17) \end{aligned}$$

and we label  $N_\phi = \delta(x)|_{x \rightarrow 0} \equiv \int d\phi / 2\pi$  as the number of laser cycles, which is formally infinite, but which we subsequently set equal to a finite value for the purpose of comparison with the pulsed result. The  $\delta$  function

$$\delta(c + 2\beta - n) = \delta \left[ \frac{s}{2\eta_p t} \left( 1 + \frac{\xi^2}{2} + \ell_\perp^2 \right) - n \right] \quad (18)$$

fixes  $n > 0$  (where  $n$  is often interpreted as the net number of absorbed laser photons) and also gives the kinematic range of

the  $n$ th harmonic [4],  $0 < s < s_{i,n}$ , where

$$s_{i,n} = \frac{2n\eta_p}{2n\eta_p + 1 + \xi^2/2}. \quad (19)$$

#### 1. Linearly polarized angular spectrum

Integrating out  $s$  in Eq. (17) gives the angular dependency

$$\begin{aligned} P_{j,n} &= \frac{\alpha N_\phi}{n\eta_p^2} \int \frac{d^2 r^\perp \mathcal{L}_n^2}{(1 + \mathcal{L}_n)^2} \left[ (\ell \cdot \varepsilon_j \Gamma_{0,n} - \delta_{1j} \xi \Gamma_{1,n})^2 \right. \\ &\left. - (\Gamma_{2,n} \Gamma_{0,n} - \Gamma_{1,n}^2) \frac{\mathcal{L}_n^2 \xi^2}{4(1 + \mathcal{L}_n)} \right], \quad (20) \end{aligned}$$

where

$$\mathcal{L}_n = \frac{2n\eta_p}{(\ell^\perp)^2 + 1 + \xi^2/2} \quad (21)$$

and the arguments of the  $\Gamma$  functions have become

$$\zeta_l \rightarrow \zeta_{l,n} = \frac{\xi \mathcal{L}_n}{\eta_p} \ell \cdot \varepsilon_1, \quad \beta \rightarrow \beta_n = \frac{\xi^2 \mathcal{L}_n}{8\eta_p}.$$

#### 2. Linearly polarized light-front momentum spectrum

If Eq. (18) is used to integrate out the perpendicular photon momentum instead, we acquire

$$\begin{aligned} P_{j,n} &= \frac{\alpha N_\phi}{\eta_p} \int_0^{s_{l,n}} ds \int_{-\pi}^{\pi} d\theta_r \left[ (\ell_n \cdot \varepsilon_j \Gamma_{0,n} - \delta_{j,1} \xi \Gamma_{1,n})^2 \right. \\ &\left. - (\Gamma_{2,n} \Gamma_{0,n} - \Gamma_{1,n}^2) \frac{s^2 \xi^2}{4t} \right], \quad (22) \end{aligned}$$

where  $\ell_n \cdot \varepsilon_1 = -|\ell_n^\perp| \cos \theta_r$ ,  $\ell_n \cdot \varepsilon_2 = -|\ell_n^\perp| \sin \theta_r$ , and we define  $|\ell_n^\perp| = \sqrt{2n\eta_p(s_{l,n} - s)/(s s_{l,n})}$ . The argument  $\zeta_l$  of the  $\Gamma$  functions becomes

$$\zeta_l \rightarrow \zeta_{l,n} = -\frac{s\xi}{t\eta_p} |\ell_n^\perp| \cos \theta_r.$$

## IV. CIRCULARLY POLARIZED PHOTON

In this section, we consider the background to be a circularly polarized field,

$$a(\phi) = m\xi g(\phi) [\varepsilon_1 \cos(\phi) + \varepsilon_2 \sin(\phi)], \quad (23)$$

which has a right-handed polarization,

$$\varepsilon_+ = \frac{1}{\sqrt{2}} (\varepsilon_1 + i\varepsilon_2).$$

The derivation is very similar to the linearly polarized case. Repeating the previous derivation and replacing the photon polarization with  $\varepsilon_\pm$ , we acquire the circularly polarized photon-momentum spectrum:

$$\begin{aligned} \frac{d^3 P_\pm}{ds d^2 r^\perp} &= \frac{\alpha}{(2\pi\eta_p)^2} \frac{s}{t} \int d\phi \int d\phi' e^{i(\phi - \phi') \langle \frac{k \cdot \pi p}{s \cdot q} \rangle} \\ &\times \frac{1}{2} \left[ \frac{s^2}{4t} \Delta + \Pi^\pm(\phi) \cdot \Pi^\pm(\phi') \right. \\ &\left. \pm i f_s \Pi^\pm(\phi) \times \Pi^\pm(\phi') \right], \quad (24) \end{aligned}$$

in which we define  $f_s = 1 + s^2/2t$ , and use the shorthand:  $x^\perp \cdot y^\perp = x^1 y^1 + x^2 y^2$  and  $x^\perp \times y^\perp = x^1 y^2 - x^2 y^1$ . We employ here the same regularization as in the linear case:  $\Pi^\perp(\phi) \rightarrow \Pi_{\text{reg}}^\perp(\phi)$ . Performing the integration over the transverse momentum, we acquire the light-front momentum spectrum:

$$\mathbf{P}_\pm = \frac{\alpha}{2\pi\eta_p} \int_0^1 ds \int d\varphi \left( \int_0^\infty \frac{d\theta}{\theta} \mathcal{K}_\pm - \frac{\pi}{2} \right), \quad (25)$$

where

$$\mathcal{K}_\pm = \left[ 1 - \frac{1}{2} f_s \Delta \pm i f_s (\mathbf{b} - \mathbf{b}^*) \right] \sin \left( \frac{s\theta\mu}{2t\eta_p} \right), \quad (26)$$

where  $\mathbf{b} = [a(\phi') - \langle a \rangle] \cdot \boldsymbol{\varepsilon}_1$   $[a(\phi) - \langle a \rangle] \cdot \boldsymbol{\varepsilon}_2/m^2$  and  $\mathbf{b}^* = [a(\phi) - \langle a \rangle] \cdot \boldsymbol{\varepsilon}_1$   $[a(\phi') - \langle a \rangle] \cdot \boldsymbol{\varepsilon}_2/m^2$ . Summing over polarizations in Eq. (25) then recovers the same polarization-averaged probability,  $\mathbf{P} = \mathbf{P}_+ + \mathbf{P}_-$ , as in the linear polarization case, Eq. (11).

### A. Photon-polarized NLC LCFA

With the same procedure as in the linear case, we acquire the LCFA result for circular polarization:

$$\begin{aligned} \frac{d^3 \mathbf{P}_\pm}{ds d^2 r^\perp} &= \frac{\alpha}{2\pi\eta_p} \int d\varphi [(2y f_s - z) \text{Ai}(y) \\ &\pm 2f_s |\xi^\perp(\varphi)|^{-1} |\Pi^\perp(\varphi) \times \xi^\perp(\varphi)| \sqrt{z} \text{Ai}'(y)], \end{aligned} \quad (27)$$

in which  $\xi^\perp(\varphi) := d^\perp(\varphi)/m$  includes the field amplitude, the direction, and the pulse envelope. In the same vein as the linearly polarized case, we can integrate over the transverse photon momenta to acquire the light-front momentum spectrum of the LCFA:

$$\frac{d\mathbf{P}_\pm}{ds} = -\frac{\alpha}{2\eta_p} \int d\varphi \left[ \text{Ai}_1(z) + 2f_s \frac{1}{z} \text{Ai}'(z) \right]. \quad (28)$$

For a constant crossed field background, when one integrates over the transverse photon momentum, one is simultaneously integrating over the trajectory of the electron since there is a one-to-one mapping between the component of photon momentum parallel to the background field and the electron's phase position [25]. Due to the symmetry of a circularly polarized background, after this integration over the trajectory, no information is retained about the polarization of the background field. Therefore the spectrum in Eq. (28) is the same for photons in different circularly polarized states (this is not the case for the angularly resolved LCFA, for the same reason). The probability changes due to scattering into different polarization states:  $\Delta \mathbf{P} = \mathbf{P}_+ - \mathbf{P}_- = 0$ . However, we note that, when the intensity of the linearly polarized laser field is twice as large as the intensity of the circularly polarized laser field, the total unpolarized probability is indeed the same for linear and circular cases ( $\mathbf{P} = \mathbf{P}_1 + \mathbf{P}_2 = \mathbf{P}_+ + \mathbf{P}_-$ ).

### B. Circularly polarized monochromatic field

The derivation is very similar to the linearly polarized monochromatic case [where now  $g(\phi) = 1$  in Eq. (23)] with the added simplification that  $a^2 = -m^2 \xi^2$  is a constant and so only one Jacobi-Anger expansion is required for each phase integration, resulting in an expression with products

of two Bessel functions (rather than products of four Bessel functions as in the linear case). We find the probability  $\mathbf{P}_\pm = \sum_{n=-\infty}^{\infty} \mathbf{P}_{\pm,n}$ , where

$$\begin{aligned} \mathbf{P}_{\pm,n} &= \frac{\alpha N_\phi}{2\eta_p^2} \int_0^1 ds \int d^2 r^\perp \frac{s}{t} \delta(c + 4\beta - n) \\ &\times \{ f_s \xi^2 / 2 (J_{n+1}^2 + J_{n-1}^2 - 2J_n^2) - J_n^2 \\ &\pm 2f_s \xi^2 [s(1 + \xi^2)/(\eta_p t) - n] J'_n J_n / \zeta_c \}, \end{aligned} \quad (29)$$

and the argument of the Bessel functions  $J_n \equiv J_n(\zeta_c)$  [ $J'_n \equiv J'_n(\zeta_c)$ ] is

$$\zeta_c = \xi |\ell^\perp| \frac{s}{\eta_p t}.$$

The  $\delta$  function again fixes the net number of absorbed laser photons  $n > 0$  and gives the kinematic range of the  $n$ th harmonic,  $0 < s < s_{c,n}$ , where

$$s_{c,n} = \frac{2n\eta_p}{2n\eta_p + 1 + \xi^2}, \quad (30)$$

which is the linear case, Eq. (19), with the substitution  $\xi^2/2 \rightarrow \xi^2$ .

#### 1. Circularly polarized angular spectrum

Evaluating the  $\delta$  function by integrating over  $s$ , we obtain the angular spectrum:

$$\begin{aligned} \frac{d^2 \mathbf{P}_{\pm,n}}{dr_x dr_y} &= \frac{\alpha N_\phi}{2\eta_p^2} \frac{C_n^2}{(1 + C_n)^2} \frac{1}{n} \\ &\times \{ f_s \xi^2 / 2 (J_{n+1}^2 + J_{n-1}^2 - 2J_n^2) - J_n^2 \\ &\pm 2f_s \xi^2 [C_n(1 + \xi^2)/\eta_p - n] J'_n J_n / \zeta_{c,n} \}, \end{aligned} \quad (31)$$

where

$$C_n = \frac{2n\eta_p}{(\ell^\perp)^2 + 1 + \xi^2},$$

and the argument of the Bessel functions becomes

$$\zeta_c \rightarrow \zeta_{c,n} = \xi |\ell^\perp| C_n / \eta_p.$$

#### 2. Circularly polarized light-front momentum spectrum

Integrating the  $\delta$  function over the transverse momentum  $r^\perp$ , we acquire the energy spectrum:

$$\begin{aligned} \frac{d\mathbf{P}_{\pm,n}}{ds} &= \frac{\pi\alpha N_\phi}{\eta_p} \left\{ \frac{f_s}{2} \xi^2 (J_{n+1}^2 + J_{n-1}^2 - 2J_n^2) - J_n^2 \right. \\ &\left. \pm 2f_s \xi^2 \left( \frac{s}{t} \frac{1 + \xi^2}{\eta_p} - n \right) \frac{1}{\zeta_{c,n}} J'_n J_n \right\}, \end{aligned} \quad (32)$$

where the argument of the Bessel functions is replaced:

$$\zeta_c \rightarrow \zeta_{c,n} = \xi |\ell_n^\perp| \frac{s}{\eta_p t}, \quad |\ell_n^\perp| = \sqrt{2n\eta_p \frac{s_{c,n} - s}{s s_{c,n}}}.$$

Summing over polarization states, we recover the unpolarized formula [60].

## V. NUMERICAL CALCULATIONS

In this section, we consider an example scenario of a head-on collision between an 8-GeV electron and an eight-cycle (full width at half maximum, 11 fs) laser pulse with intermediate intensity  $\xi = 1$  and frequency  $\omega_0 = 1.55$  eV. The corresponding pulse envelope is  $g(\phi) = \cos^2(\phi/4\sigma)$ , with  $|\phi| < 2\pi\sigma$  and  $\sigma = 4$ , and the electron energy parameter is  $\eta_p = 0.095$ . This choice of parameters is motivated by upcoming high-energy experiments such as LUXE and E320. In this parameter region, the scattered photons are collimated in the electron incident direction with a very small angular spread. We refer to  $\epsilon_1$  and  $\epsilon_+$  as “ $E$ -polarization” states, because they are almost parallel to background fields with polarization  $\epsilon_1$  and  $\epsilon_+$  in the linear and circular cases, respectively [almost parallel, because photons are emitted with finite (small) angles].  $\epsilon_2$  and  $\epsilon_-$  are then referred to as “ $B$ -polarization” states, as they are (almost) parallel to the magnetic field in each case. The polarization purity is defined as the fraction of the  $E$ -polarized photons:  $\mathcal{P} = P_1/P$  in the linear case and  $\mathcal{P} = P_+/P$  in the circular case. For the  $n$ th order of harmonic, the polarization purity is  $\mathcal{P}_n = P_{1,n}/(P_{1,n} + P_{2,n})$  in the linear case and  $\mathcal{P}_n = P_{+,n}/(P_{+,n} + P_{-,n})$  in the circular case.

### A. Linearly polarized background

Figure 1 shows the energy spectra of the polarized photons and the behavior of the polarization purity for different values of  $s$  in the linear background field. As shown in Fig. 1(a), the relative values of the polarized spectra depend sensitively on the photon light-front momentum  $s$ : in the low-energy limit  $s \rightarrow 0$ , the photons are unpolarized ( $\mathcal{P} = 0.5$ ) as shown in Fig. 1(b). However, in the high-energy region, starting around the Compton edge [vertical black line in Fig. 1(a), the kinematic bound of the first harmonic  $s_{1,1}$ ], photons are more likely to be scattered into the  $E$ -polarization state, reaching a high purity  $>90\%$ .

An evident harmonic structure can be observed in the photons’ energy spectra in Fig. 1(a) for the eight-cycle laser pulse. The harmonic structure corresponds to the multippeak structure in the polarization purity [red solid line in Fig. 1(b)]. To illustrate this, we plot the polarization purity (blue dash-dotted line) from a monochromatic background, which broadly agrees with the pulsed result. We can also see that the highest purity (about 95%) results from the first harmonic, which is dominant in the  $E$ -polarization state and becomes purely  $E$ -polarized at the Compton edge. For higher-order harmonics, the polarization purity becomes smaller, and in the low light-front momentum region it can even display a dominance of  $B$ -polarized photons where  $\mathcal{P} < 0.5$ , for  $\mathcal{P}_{2,3}$  in Fig. 1(b).

In Fig. 2, we show the angular spectra of the polarized photons,  $d^2P/dr_x dr_y$ , for the same parameters as in Fig. 1. [Only photons with  $0 < s < 0.4$  have been included as higher values of  $s$  are strongly suppressed for these parameters, as shown in Fig. 1(a)]. We observe that  $E$ -polarized photons are tightly collimated with the incident electron propagation direction ( $r^\perp = 0$ ) with an angular spread:  $2|r^\perp|/\gamma_p \sim 2\xi/\gamma_p \approx 0.13$  mrad. This is much narrower than the  $B$ -polarized photons’ distribution, and with the peak value 1 order of magnitude larger than that of the  $B$ -polarized photons. We

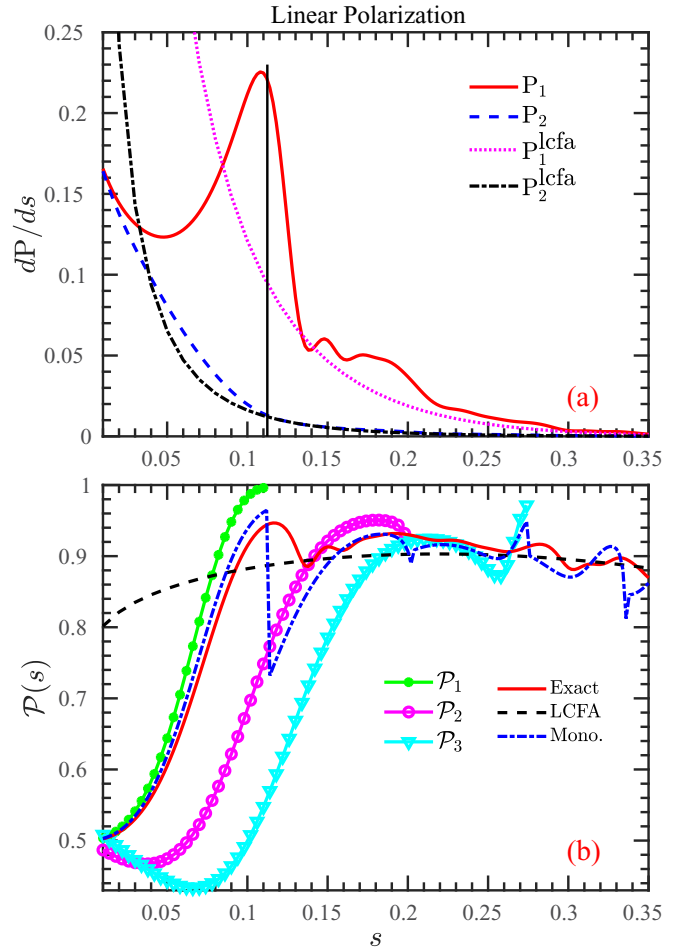


FIG. 1. (a) Polarized energy spectra: Exact QED results and LCFA results. The black vertical solid line denotes the upper limit of the first harmonic  $s_{1,1}$  from Eq. (19). (b) Polarization purity: Exact QED results, LCFA results, and monochromatic results. The markers denote the polarization purity of the first three harmonics  $\mathcal{P}_n$ . Head-on collision is considered with the following parameters:  $\xi = 1$  and  $\omega_0 = 1.55$  eV.

also see that the  $B$ -polarized photons are scattered in a four-peak quadrupole distribution, while the  $E$ -polarized photons are scattered into the typical dipole-radiation distribution. In order to compare with the monochromatic results, we pick a scaling factor  $N_\phi$  by replacing the integration over the phase with an integral over the pulse envelope,  $N_\phi = \int d\phi/2\pi \rightarrow \int d\phi g(\phi)/2\pi = 4$ . In Figs. 2(c) and 2(d), we see good quantitative agreement with the pulsed results and also that the multipole structure is clearly reproduced.

The significant difference in the angular distribution of the polarized photons results in the particular structure in the distribution of the photon polarization purity shown in Fig. 3(a). Around the electron incident direction,  $|r^\perp| < 0.5$  corresponding to the photon angular spread of  $\sim 0.064$  mrad, we can achieve an almost purely  $E$ -polarized ( $\mathcal{P} > 96\%$ ) photon beam, and for a broader angular spread of  $\sim 0.1$  mrad, photons are emitted with the polarization purity of 85%. Here we want to emphasize that because high-energy photons are tightly collimated in the electron incident direction, a highly

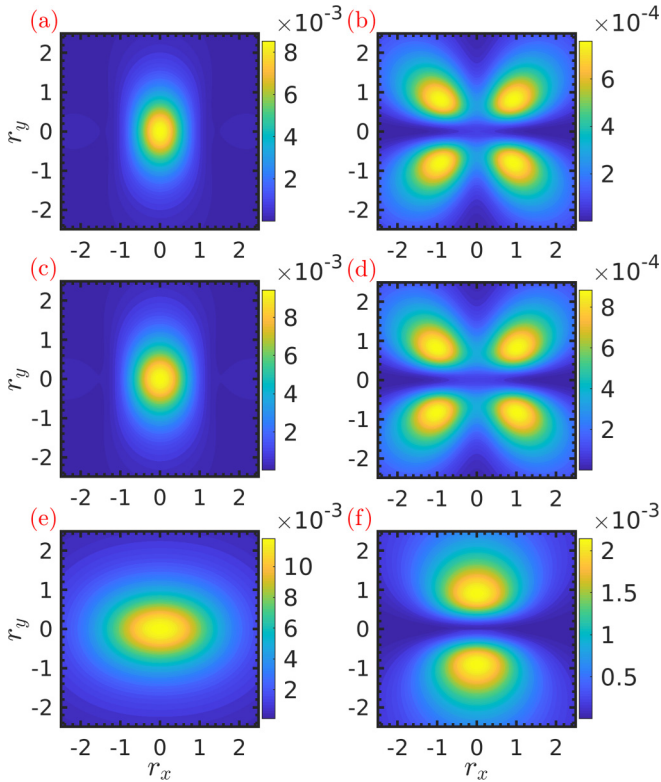


FIG. 2. Angular distribution  $d^2P/dr_x dr_y$  of the linearly polarized photons. Left column:  $E$  polarization. Right column:  $B$  polarization. Upper panels (a) and (b): Exact QED calculation for a pulse. Central panels (c) and (d): QED calculation for a monochromatic field. We take  $N_\phi = 4$ . Bottom panels (e) and (f): The LCFA results. The axes  $r_{x,y}$  are dimensionless and relate directly to the scattering angle of the photon [see Eq. (5)]. The parameters are the same as those used in Fig. 1.

$E$ -polarized  $\gamma$ -ray can be generated if we exclude the photons with a large scattering angle [66].

For comparison, we also show the corresponding LCFA results in Figs. 1, 2, and 3. As expected [29], in this intermediate-energy region, LCFA cannot reproduce the harmonic structure in the spectra and therefore cannot be used in this regime to give an accurate prediction of the purity of the emitted photons. As shown in Fig. 1, for lower-energy

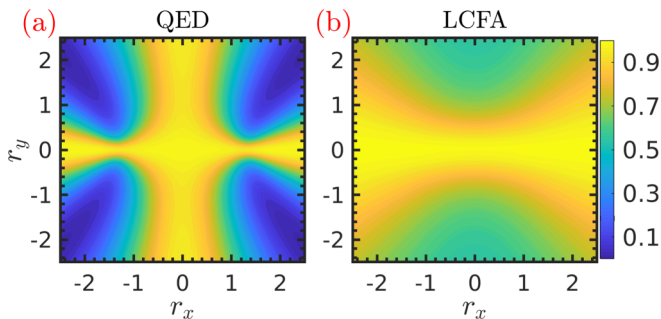


FIG. 3. Angular distribution of the polarization purity  $\mathcal{P}$  in a linearly polarized background. (a) The exact QED calculation for a pulse. (b) The LCFA results. The parameters are the same as those used in Fig. 1.

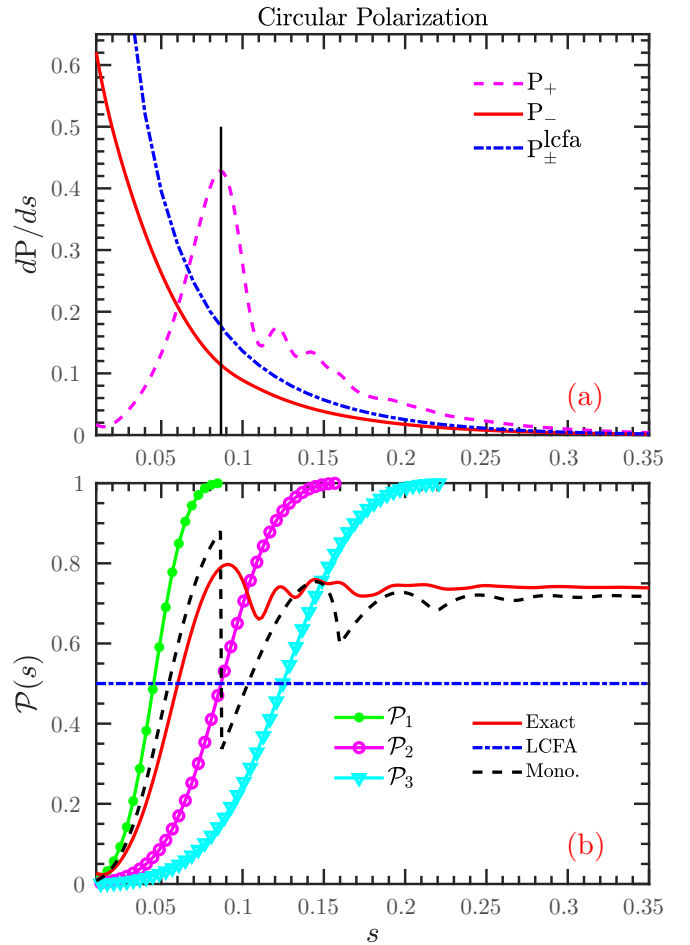


FIG. 4. (a) Polarized energy spectra: Exact QED results and LCFA results. The black vertical solid line denotes the upper limit of the first harmonic  $s_1$  from Eq. (30). (b) Polarization purity: Exact QED results, LCFA results, and monochromatic results. The markers denote the polarization purity of the first three harmonics  $\mathcal{P}_n$ . The parameters are the same as those as in Fig. 1.

photons,  $s \rightarrow 0$ , the LCFA prediction for  $dP/ds$  diverges, as is well known, and hence it overestimates the polarization purity. For higher-energy photons, the LCFA result averages through the harmonic structure. We can also see that the angularly resolved LCFA result shows large deviations from the exact QED calculations shown in Fig. 2. The LCFA broadens the angular distribution of  $E$ -polarized photons and merges the four-peak structure in the distribution of the  $B$ -polarized photons into a double-peak structure. Therefore, the LCFA predicts a significantly different polarization purity distribution in Fig. 3. As the LCFA result overestimates the peak value of the photon distribution, especially for the  $B$ -polarized photons, the value of the polarization purity in the  $y$  direction (perpendicular to the field polarization direction) is underestimated.

## B. Circularly polarized background

Figure 4(a) shows the energy spectra of the circularly polarized photons in a circularly polarized background field. Unlike in a linearly polarized background, the lower-energy

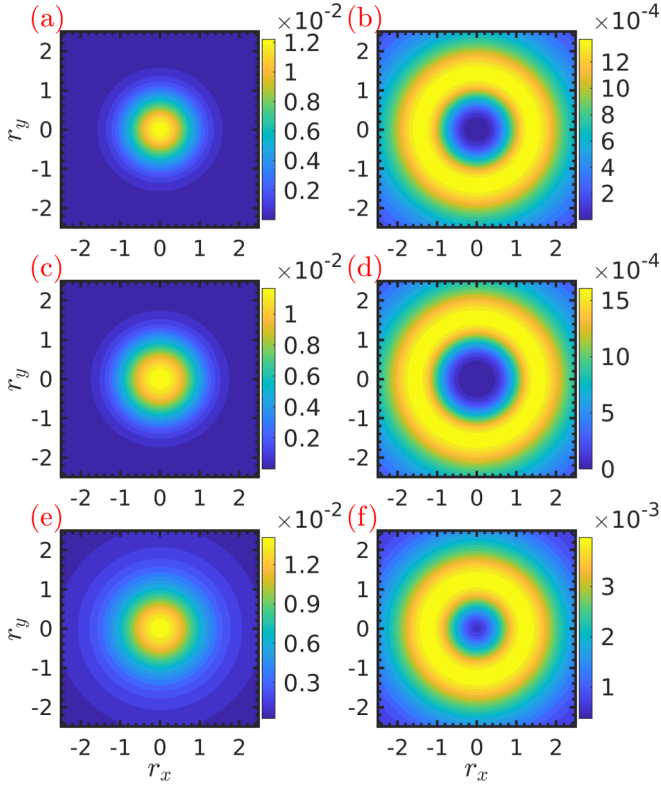


FIG. 5. Angular distribution  $d^2\mathcal{P}/dr_x dr_y$  of the circularly polarized photons. Left column:  $E$  polarization. Right column:  $B$  polarization. Upper panels (a) and (b): Exact calculation for a pulse. Central panels (c) and (d): Calculation for a monochromatic field ( $N_\phi = 4$ ). Bottom panels (e) and (f): The LCFA results. Photons are included in the range  $0 < s < 0.4$ , and the parameters are the same as those in Fig. 4.

photons,  $s \rightarrow 0$ , are purely  $B$ -polarized,  $\mathcal{P} \rightarrow 0$ , whereas higher-energy photons, with  $s \gtrsim s_{c,1}$  [ $s_{c,1}$  is the Compton edge, vertical black line in Fig. 4(a)], are highly polarized in the  $E$ -polarization state. Thus the polarization purity increases from  $\mathcal{P} = 0$  at the low-energy limit up to  $\mathcal{P} > 70\%$  in the higher-energy region as shown in Fig. 4(b). This tendency can be explained via the monochromatic result, which as shown in Fig 4(b) (black dash-dotted line), matches well with the pulse result (red solid line). This change in the polarization purity as  $s$  is increased from 0 can be explained mathematically. From Eq. (32), the perturbative expansion relation for a small argument of the Bessel function,  $J_n(\xi) \sim \xi^n$ , can be used to show that in the  $s \rightarrow 0$  limit for the  $n$ th order of harmonic gives  $d\mathcal{P}_{\pm,n}/ds \sim 2f_s \xi_0 (n^2 \mp n^2) \xi_{c,n}^{2n-2}$ , whereas in the  $s \rightarrow s_{c,n}$  limit,  $d\mathcal{P}_{\pm,n}/ds \sim 2f_s \xi_0 (n^2 \pm n^2) \xi_{c,n}^{2n-2}$ . Thus the harmonics are purely  $B$ -polarized ( $\mathcal{P}_n = 0$ ) at  $s \rightarrow 0$  and purely  $E$ -polarized ( $\mathcal{P}_n = 1$ ) at the harmonic bound  $s \rightarrow s_{c,n}$ , as also shown in Fig 4(b). Furthermore, the low polarization purity of each harmonic at  $s \ll s_{c,n}$  reduces the purity of the sum of all the harmonics and finally results in the lower polarization purity at larger  $s$  in the circular case than in the linear case.

In Fig. 5, we present the angular distribution of the polarized photons. As shown, the azimuthal symmetry is maintained in an eight-cycle pulse. Similar to the linear case, the  $E$ -

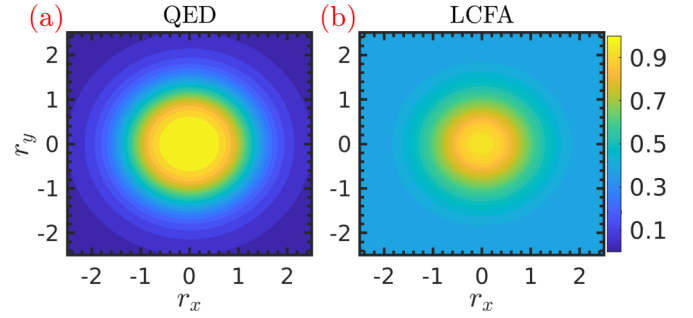


FIG. 6. Angular distribution of the polarization purity in the circularly polarized background. (a) The exact QED calculation for a pulse. (b) The LCFA results. The parameters are the same as those used in Fig. 4.

polarized photons are more collimated in the electron incident direction with an angular spread of  $2|r^\perp|/\gamma_p \sim 2\xi/\gamma_p \approx 0.13$  mrad, and the distribution peak value is 1 order of magnitude larger than that of the  $B$ -polarized photons. In Fig. 6, we plot how the polarization purity depends on the scattering angle. We observe that the photons scattered with the smallest angle have the highest purity. For the current parameters, within an angular spread of  $< 0.077$  mrad the scattered photons are almost purely  $E$ -polarized with  $\mathcal{P} > 96\%$ , and within an angular spread of  $\sim 0.1$  mrad they have a purity of  $\mathcal{P} \sim 88\%$ . Alternatively, we could concentrate on large-angle scattering and find that, for angles  $> 0.33$  mrad, photons are highly  $B$ -polarized ( $\mathcal{P} < 5\%$ ) instead.

In Figs. 4, 5, and 6, we also show the LCFA results for comparison. Away from the center of the distribution in Fig. 6, the LCFA predicts a polarization purity of 0.5, which is equal to the ratio one acquires after integrating out transverse photon momenta, and shows that the LCFA cannot resolve the polarization state of wide-angle scattering. In the center of the distribution, we see that the LCFA predicts a narrower peak than the QED result, suggesting that the actual situation is more favorable in this regime than simulations based on the LCFA would predict. Because the LCFA result overestimates the value of the  $B$ -polarized photon distribution, the peak value of the polarization purity in Fig. 6 is underestimated to be less than the exact QED value:  $\mathcal{P} < 96\%$ .

## VI. CLASSICAL ANALYSIS

In Figs. 2(a) and 2(d), we observe the multipole-radiation structure in the angular spectra of the polarized photons. To show this structure more clearly, we present the angular distribution of the first three harmonics in Fig. 7. As shown, the angular distributions of the different harmonics display different orders of multipole radiation [67].

In order to interpret the origin of the orbital-type shapes in the angular spectra, which persist when the quantum parameter  $\chi_p \ll 1$ , we perform a classical calculation of nonlinear Thomson scattering. The classical analog of the differential probability of photon emission,  $d^3\mathcal{P}^{\text{cl.}}/dk^3$ , is given by the energy of the emitted field in units of frequency:

$$\frac{d^3\mathcal{P}^{\text{cl.}}}{dk^3} = \frac{1}{k^0} \frac{d^3P^0}{dk^3},$$

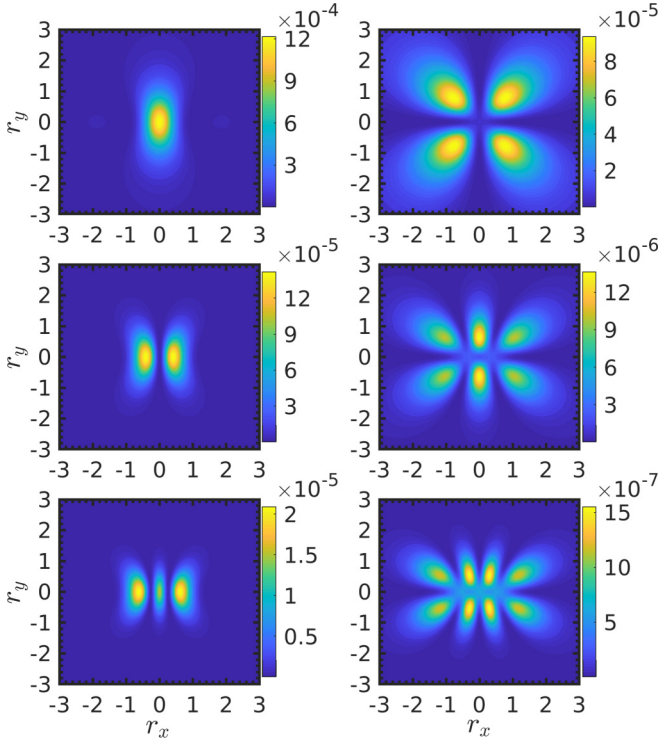


FIG. 7. Angular spectra  $d^2P_{j,n}/dr_x dr_y$  of the first three harmonics in the linearly polarized monochromatic field:  $\xi = 1$  and  $\eta_p = 0.095$  (8-GeV electrons). Left column:  $E$  polarization. Right column:  $B$  polarization. Upper panels: First harmonic. Central panels: Second harmonic. Bottom panels: Third harmonic.

where  $P^\mu$  is the four-momentum of the field emitted by the electron through interaction with the electromagnetic background. Proceeding from Coleman [68], we write

$$P^{\text{cl.}} = \frac{2}{(2\pi)^3} \int d^4k \tilde{j}_\lambda^*(k) \tilde{j}^\lambda(k) \theta(k^0) \delta(k^2), \quad (33)$$

where  $\tilde{j} = \int d^4x j(x) \exp[ik \cdot x]$  and we use a definition for the classical current of  $j^\mu(x) = e \int \delta^{(4)}[x - x'(s)] \pi'^\mu(\tau) d\tau$ , where  $\tau$  is the proper time, related to the external-field phase by  $d\tau/d\varphi = (m\eta_p)^{-1}$ . This then leads to

$$P^{\text{cl.}} = \frac{\alpha}{\pi^2 \eta_p^2} \int \frac{ds d^2k^\perp}{2s} d\varphi d\varphi' \pi(\varphi) \cdot \pi(\varphi') e^{ik \cdot [x(\varphi) - x(\varphi')]}. \quad (34)$$

At this point, we decompose the trajectory using the basis introduced in Eq. (2) and the derivation is then very similar to the QED version. The total probability can be written as  $P^{\text{cl.}} = P_1^{\text{cl.}} + P_2^{\text{cl.}}$ , where  $P_j^{\text{cl.}} = \sum_n P_{j,n}^{\text{cl.}}$  and

$$P_j^{\text{cl.}} = \frac{2\alpha}{\eta_p} \int \frac{d\varphi}{2\pi} \int ds ds' r^\perp \delta(\tilde{c} + 2\tilde{\beta}_s - n) \times \{ \delta_{j,2}(r \cdot \varepsilon_2)^2 \Gamma_{0,n}^2 + \delta_{j,1} [ (r \cdot \varepsilon_1)^2 \Gamma_{0,n}^2 + 2m\xi r \cdot \varepsilon_1 \Gamma_{1,n} \Gamma_{0,n} + \xi^2 \Gamma_{1,n}^2 ] \}, \quad (35)$$

where the arguments of the  $\Gamma_{l,n}$  functions are now

$$\tilde{\alpha}_s = \frac{\xi s}{\eta_p} r \cdot \varepsilon, \quad \tilde{\beta}_s = \frac{\xi^2 s}{8\eta_p}.$$

We note that energy-momentum conservation is different in the classical case, because the electron experiences no recoil classically. This is reflected by the modified  $\delta$ -function argument:

$$\delta(\tilde{c} + 2\tilde{\beta}_s - n) = \delta \left[ \frac{s}{2\eta_p} \left( 1 + \frac{\xi^2}{2} + (\mathbf{r}^\perp)^2 \right) - n \right],$$

which on comparison with the quantum version Eq. (18) has been modified by a replacement  $s/(1-s) \rightarrow s$ . (Recalling that the scattered electron energy parameter  $\eta_q = \eta_p(1-s)$ , we see that setting  $1-s \rightarrow 1$  is equivalent to neglecting the electron recoil). There is also an extra term in the classical integrand which originates from the  $e_\pm$  directions, of the form

$$[1 + (\mathbf{r}^\perp)^2] \Gamma_{0,n}^2 - 2\xi r \cdot \varepsilon_1 \Gamma_{0,n} \Gamma_{1,n} + \xi^2 \Gamma_{0,n} \Gamma_{2,n},$$

but this disappears, because it is a boundary term in the integration over  $\phi$  and  $\phi'$  (it is proportional to  $k \cdot \pi$ , which occurs in the exponent).

One immediate consequence arises in the angular spectrum when  $s$  is integrated over in Eq. (36):

$$P_j^{\text{cl.}} = \frac{2\alpha}{\eta_p} \int \frac{d\varphi}{2\pi} \int_0^{2\pi} \frac{d\theta_r}{2\pi} \int_{r_n}^\infty dr r s_n^* \{ \delta_{j,2} (\mathbf{r}^\perp \cdot \varepsilon_2)^2 \Gamma_{0,n}^2 + \delta_{j,1} [ (\mathbf{r}^\perp \cdot \varepsilon_1)^2 \Gamma_{0,n}^2 - 2m\xi \mathbf{r}^\perp \cdot \varepsilon_1 \Gamma_{1,n} \Gamma_{0,n} + \xi^2 \Gamma_{1,n}^2 ] \}, \quad (36)$$

where  $s_n^* = y_n^*$  from Eq. (21). However, because there is no electron recoil in the classical description,  $s_n^* \leq 1$ , whereas the equivalent QED parameter,  $y_n^*$ , is unbounded. This means that there exists a classical ‘‘angular edge’’ in analogy with the Compton edge [4] but in the angular spectrum:

$$r_n = \theta(u_n) \sqrt{u_n}, \quad u_n = 2n\eta_p - 1 - \xi^2/2. \quad (37)$$

Therefore, the smoothing of the angular harmonic edges is a quantum effect.

Upon comparison with the quantum version for the total probability, Eq. (22), we note two further differences. First, the decomposition that we have made to the electron’s trajectory, by projecting the instantaneous *electron momentum* onto the directions  $\varepsilon_{1,2}$ , matches the decomposition in the quantum case,  $\varepsilon_{1,2}$  of the *photon polarization*. This mainly originates from the choice of polarization basis, in which  $p \cdot \varepsilon_1 = r \cdot \varepsilon_1$  and  $p \cdot \varepsilon_2 = r \cdot \varepsilon_2$ . We see thereby the mapping between the classical electron’s motion and the polarization of the emitted photon in the QED case. The second difference, is that there are terms from QED that are absent in the classical formula, in particular the term

$$-2(m\xi)^2 \frac{s^2}{4(1-s)} [\Gamma_{2,n} \Gamma_{0,n} - \Gamma_{1,n}^2].$$

This term is of purely quantum origin, which is made manifest when we recall that  $s = \eta_k/\eta_p = \varkappa \cdot k/\varkappa \cdot p \propto \hbar$ , and so when we take the limit of  $\hbar \rightarrow 0$  of the quantum expression, this term disappears. (Incidentally, the other terms survive, because we have the combination  $\eta_p^{-1} \int ds$ , which survives in the limit of  $\hbar \rightarrow 0$ .)

The angular harmonic spectrum of photons emitted with polarization perpendicular to the field resembles the spherical harmonic decomposition of the Green’s function of the wave equation from classical electrodynamics [67]. A connection to this expansion can be made by noting that the leading term

dictating the shape of the angular harmonics is given by  $\Gamma_{0,n}^2$ , where

$$\Gamma_{0,n} = \sum_{t=-\infty}^{\infty} J_t\left(\frac{\xi^2 s}{8\eta_p}\right) J_{2t+n}\left(\frac{\xi s r \cos\theta}{\eta_p}\right). \quad (38)$$

For the lowest harmonics,  $s \ll 1$  and our analysis leads to the highest polarization purities when  $\xi/\eta_p$  is not too large, so the Bessel arguments are, in general, small. It turns out that the limit [69]

$$J_n(z) = \lim_{m \rightarrow \infty} m^n P_m^{-n}\left(\cos \frac{z}{m}\right), \quad (39)$$

where  $P_m^{-n}$  are the associated Legendre polynomials, is already well approximated for a small argument  $|z| \ll 1$  at  $m = 1$ . Then we see that the leading term can be approximated by

$$\Gamma_{0,n} = \sum_{t=-\infty}^{\infty} J_t\left(\frac{\xi^2 s}{8\eta_p}\right) P_1^{-(2t+n)} \left[1 - \left(\frac{\xi s r \cos\theta}{\eta_p}\right)^2\right]. \quad (40)$$

Upon comparison with the form of the spherical harmonics,

$$Y_l^m(\theta, \phi) = N e^{im\phi} P_l^m(\cos\theta), \quad (41)$$

and noting that  $P_l^{-m} \propto P_l^m$ , we see that each higher-harmonic  $n$  is associated with a higher value of the index  $m$ .

## VII. CONCLUSION

We investigated the polarization of a photon generated by nonlinear Compton scattering of an electron in a plane-wave background. Our analysis considers the generation of linearly polarized and circularly polarized photons in correspondingly polarized background fields. We considered a finite pulse, a monochromatic background, and the locally constant field approximation (LCFA) for each polarization case. The light-front momentum and angularly resolved spectra for each case were presented.

Motivated by the upcoming high-energy experiments LUXE at DESY and E320 at FACET-II, we focused attention on having a plane-wave laser pulse of intermediate-intensity parameter  $\xi = 1$ . We found that the harmonic structure of the photon spectrum is reflected in the polarization purity of the scattered photons. The angular spectrum of emitted photons is substantially different for photons polarized parallel to the electric field ( $E$ -polarized) to the angular spectrum of photons polarized parallel to the magnetic field ( $B$ -polarized), in both linearly and circularly polarized cases. By performing a classical calculation for the equivalent process of nonlinear Thomson scattering, we identified an explanation for the different angular distribution of different photon polarization states due to the motion of the electron in a plane-wave background in the electric- and magnetic-field directions.

Approaches based on the LCFA (which is the main method by which quantum effects are included in numerical simulations of high-intensity laser-matter interactions) cannot reproduce the structure of the angular distributions at intermediate intensities. In particular, for the linearly polarized case, the multipole structure is beyond local approaches, and for the circularly polarized case, the spherical harmonic structure is beyond local approaches. The LCFA approach is thus

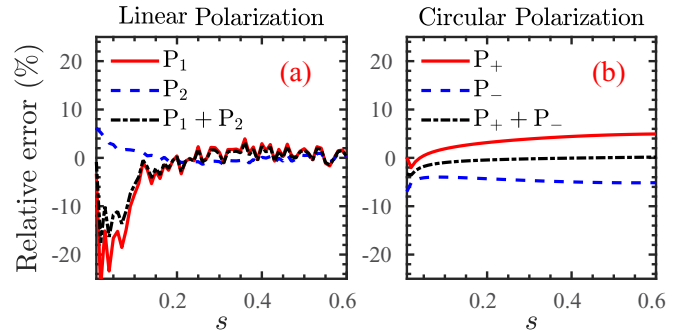


FIG. 8. Relative error  $(dP_j/ds - dP_j^{\text{lcfa}}/ds)/(dP_j/ds)$  in the energy spectra of each LCFA result  $dP_j^{\text{lcfa}}/ds$  compared with the corresponding monochromatic result  $dP_j/ds$  in the region  $0.01 < s < 0.6$ . The parameters are  $\xi = 8$  and  $\eta_p = 0.095$ .

incapable of describing the angular distribution of the photon polarization purity in the parameter regime of interest in high-energy experiments at intermediate field intensity. The LCFA also performs poorly at predicting the yield of photons with a given polarization in the low-energy part of the spectrum as well as around the first harmonic (the Compton edge), which is an identified experimental observable of interest [20].

This naturally raises the question as to whether one should use the polarized LCFA or the unpolarized LCFA to describe the dynamics of QED cascades. To answer this, we would first point out that QED cascades driven by the laser field are necessarily in the high-intensity regime, whereas in the current paper, we are concerned with the intermediate intensity regime of  $\xi \sim O(1)$ . Therefore, the error in the different LCFAs will be reduced. Second, in each link of the cascade it is usually assumed to be a good approximation that this emission is forward; i.e., the angular spread we have calculated here for each polarization case is not resolved. In Fig. 8, we compare the relative error in the energy spectra of each polarized LCFA with the unpolarized LCFA, for  $\xi = 8$  and  $\eta_p = 0.095$ .

As one can see, in the linearly polarized case, the relative error of the LCFAs is very similar and rather low (at small  $s$ , the relative error can be about a factor 20% larger, but this is not usually the parameter range of interest in cascades). In a circularly polarized background, although the difference in the error grows with  $s$ , it remains rather small over the entire spectrum at around 5%. Therefore, the photon-polarized LCFA describes QED cascade dynamics to a level of accuracy similar to that of the unpolarized LCFA.

We finish by highlighting that, at intermediate intensities, the significant difference in the angular and energy dependency of  $E$ - and  $B$ -polarized photons lends itself to the possibility of generating highly brilliant, highly polarized sources of  $\gamma$  photons, as explored in Ref. [66].

## ACKNOWLEDGMENTS

S.T. and B.K. are supported by the U.K. Engineering and Physical Sciences Research Council, Grant No. EP/S010319/1.

- [1] A. I. Nikishov and V. I. Ritus, *Sov. Phys. JETP* **19**, 529 (1964).
- [2] L. S. Brown and T. W. B. Kibble, *Phys. Rep.* **133**, A705 (1964).
- [3] D. Yu. Ivanov, G. L. Kotkin, and V. G. Serbo, *Eur. Phys. J. C* **36**, 127 (2004).
- [4] C. Harvey, T. Heinzl, and A. Ilderton, *Phys. Rev. A* **79**, 063407 (2009).
- [5] M. Boca and V. Florescu, *Phys. Rev. A* **80**, 053403 (2009).
- [6] F. Mackenroth, A. Di Piazza, and C. H. Keitel, *Phys. Rev. Lett.* **105**, 063903 (2010).
- [7] T. Heinzl, D. Seipt, and B. Kämpfer, *Phys. Rev. A* **81**, 022125 (2010).
- [8] F. Mackenroth and A. Di Piazza, *Phys. Rev. A* **83**, 032106 (2011).
- [9] D. Seipt and B. Kämpfer, *Phys. Rev. A* **83**, 022101 (2011).
- [10] N. V. Elkina, A. M. Fedotov, I. Y. Kostyukov, M. V. Legkov, N. B. Narozhny, E. N. Nerush, and H. Ruhl, *Phys. Rev. Spec. Top.—Accel. Beams* **14**, 054401 (2011).
- [11] B. King, N. Elkina, and H. Ruhl, *Phys. Rev. A* **87**, 042117 (2013).
- [12] C. Ridgers, J. G. Kirk, R. Duclous, T. Blackburn, C. Brady, K. Bennett, T. Arber, and A. Bell, *J. Comput. Phys.* **260**, 273 (2014).
- [13] D. Green and C. Harvey, *Comput. Phys. Commun.* **192**, 313 (2015).
- [14] A. Gonoskov, S. Bastrakov, E. Efimenko, A. Ilderton, M. Marklund, I. Meyerov, A. Muraviev, A. Sergeev, I. Surmin, and E. Wallin, *Phys. Rev. E* **92**, 023305 (2015).
- [15] C. Bula, K. T. McDonald, E. J. Prebys, C. Bamber, S. Boege, T. Kotseroglou, A. C. Melissinos, D. D. Meyerhofer, W. Ragg, D. L. Burke *et al.* *Phys. Rev. Lett.* **76**, 3116 (1996).
- [16] C. Bamber, S. J. Boege, T. Koffas, T. Kotseroglou, A. C. Melissinos, D. D. Meyerhofer, D. A. Reis, W. Ragg, C. Bula, K. T. McDonald *et al.*, *Phys. Rev. D* **60**, 092004 (1999).
- [17] J. M. Cole, K. T. Behm, E. Gerstmayr, T. G. Blackburn, J. C. Wood, C. D. Baird, M. J. Duff, C. Harvey, A. Ilderton, A. S. Joglekar *et al.*, *Phys. Rev. X* **8**, 011020 (2018).
- [18] K. Poder, M. Tamburini, G. Sarri, A. Di Piazza, S. Kuschel, C. D. Baird, K. Behm, S. Bohlen, J. M. Cole, D. J. Corvan *et al.*, *Phys. Rev. X* **8**, 031004 (2018).
- [19] The FACET-II SFQED Collaboration, Probing strong-field QED at FACET-II (SLAC E-320) (unpublished).
- [20] H. Abramowicz *et al.*, [arXiv:1909.00860](https://arxiv.org/abs/1909.00860).
- [21] B. King, *Phys. Rev. A* **91**, 033415 (2015).
- [22] D. Del Sorbo, D. Seipt, T. G. Blackburn, A. G. R. Thomas, C. D. Murphy, J. G. Kirk, and C. P. Ridgers, *Phys. Rev. A* **96**, 043407 (2017).
- [23] D. D. Sorbo, D. Seipt, A. G. R. Thomas, and C. P. Ridgers, *Plasma Phys. Controlled Fusion* **60**, 064003 (2018).
- [24] Y.-F. Li, R. Shaisultanov, K. Z. Hatsagortsyan, F. Wan, C. H. Keitel, and J.-X. Li, *Phys. Rev. Lett.* **122**, 154801 (2019).
- [25] V. I. Ritus, *J. Russ. Laser Res.* **6**, 497 (1985).
- [26] C. N. Harvey, A. Ilderton, and B. King, *Phys. Rev. A* **91**, 013822 (2015).
- [27] A. Di Piazza, M. Tamburini, S. Meuren, and C. H. Keitel, *Phys. Rev. A* **98**, 012134 (2018).
- [28] A. Di Piazza, M. Tamburini, S. Meuren, and C. H. Keitel, *Phys. Rev. A* **99**, 022125 (2019).
- [29] A. Ilderton, B. King, and D. Seipt, *Phys. Rev. A* **99**, 042121 (2019).
- [30] A. Ilderton, B. King, and A. J. MacLeod, *Phys. Rev. D* **100**, 076002 (2019).
- [31] A. Di Piazza, K. Z. Hatsagortsyan, and C. H. Keitel, *Phys. Rev. Lett.* **105**, 220403 (2010).
- [32] Y.-F. Li, R. Shaisultanov, Y.-Y. Chen, F. Wan, K. Z. Hatsagortsyan, C. H. Keitel, and J.-X. Li, *Phys. Rev. Lett.* **124**, 014801 (2020).
- [33] T. N. Wistisen and A. Di Piazza, *Phys. Rev. D* **100**, 116001 (2019).
- [34] V. I. Ritus, *Nucl. Phys. B* **44**, 236 (1972).
- [35] V. N. Baier, V. M. Katkov, and V. M. Strakhovenko, *Sov. Phys. Nucl. Phys.* **14**, 572 (1972).
- [36] B. King and H. Ruhl, *Phys. Rev. D* **88**, 013005 (2013).
- [37] B. King and A. M. Fedotov, *Phys. Rev. D* **98**, 016005 (2018).
- [38] V. Dinu and G. Torgrimsson, *Phys. Rev. D* **97**, 036021 (2018).
- [39] D. L. Burke, R. C. Field, G. Horton-Smith, J. E. Spencer, D. Walz, S. C. Berridge, W. M. Bugg, K. Shmakov, A. W. Weidemann, C. Bula *et al.*, *Phys. Rev. Lett.* **79**, 1626 (1997).
- [40] H. Hu, C. Müller, and C. H. Keitel, *Phys. Rev. Lett.* **105**, 080401 (2010).
- [41] A. Ilderton, *Phys. Rev. Lett.* **106**, 020404 (2011).
- [42] F. Mackenroth and A. Di Piazza, *Phys. Rev. D* **98**, 116002 (2018).
- [43] D. A. Morozov and V. I. Ritus, *Nucl. Phys. B* **86**, 309 (1975).
- [44] D. Seipt and B. Kämpfer, *Phys. Rev. D* **85**, 101701(R) (2012).
- [45] V. Dinu and G. Torgrimsson, *Phys. Rev. D* **102**, 016018 (2020).
- [46] A. M. Fedotov, N. B. Narozhny, G. Mourou, and G. Korn, *Phys. Rev. Lett.* **105**, 080402 (2010).
- [47] E. N. Nerush, I. Y. Kostyukov, A. M. Fedotov, N. B. Narozhny, N. V. Elkina, and H. Ruhl, *Phys. Rev. Lett.* **106**, 035001 (2011).
- [48] A. A. Mironov, N. B. Narozhny, and A. M. Fedotov, *Phys. Lett. A* **378**, 3254 (2014).
- [49] E. Gelfer, A. A. Mironov, A. M. Fedotov, V. F. Bashmakov, E. N. Nerush, I. Y. Kostyukov, and N. B. Narozhny, *Phys. Rev. A* **92**, 022113 (2015).
- [50] A. Gonoskov, A. Bashinov, S. Bastrakov, E. Efimenko, A. Ilderton, A. Kim, M. Marklund, I. Meyerov, A. Muraviev, and A. Sergeev, *Phys. Rev. X* **7**, 041003 (2017).
- [51] M. Tamburini, A. Di Piazza, and C. H. Keitel, *Sci. Rep.* **7** (2017).
- [52] A. Ilderton and M. Marklund, *J. Plasma Phys.* **82** (2016).
- [53] B. King and N. Elkina, *Phys. Rev. A* **94**, 062102 (2016).
- [54] Y. Nakamiya and K. Homma, *Phys. Rev. D* **96**, 053002 (2017).
- [55] S. Bragin, S. Meuren, C. H. Keitel, and A. Di Piazza, *Phys. Rev. Lett.* **119**, 250403 (2017).
- [56] J. S. Toll, Ph.D. thesis, Princeton University, 1952.
- [57] T. N. Wistisen, *Phys. Rev. D* **101**, 076017 (2020).
- [58] B. King and T. Heinzl, *High Power Laser Sci. Eng.* **4**, e5 (2016).
- [59] V. N. Baier, A. I. Mil'shtein, and V. M. Strakhovenko, *Sov. Phys. JETP* **42**, 961 (1976).
- [60] V. B. Berestetskii, E. M. Lifshitz, and L. P. Pitaevskii, *Quantum Electrodynamics*, 2nd ed. (Butterworth-Heinemann, Oxford, 1982).
- [61] V. M. Katkov and V. N. Baier, *Electromagnetic Processes at High Energies in Oriented Single Crystals* (World Scientific, Singapore, 1994).

- [62] V. Dinu, T. Heinzl, A. Ilderton, M. Marklund, and G. Torgrimsson, *Phys. Rev. D* **89**, 125003 (2014).
- [63] V. Dinu, C. Harvey, A. Ilderton, M. Marklund, and G. Torgrimsson, *Phys. Rev. Lett.* **116**, 044801 (2016).
- [64] D. Seipt, [arXiv:1701.03692](https://arxiv.org/abs/1701.03692).
- [65] V. Dinu, *Phys. Rev. A* **87**, 052101 (2013).
- [66] S. Tang, B. King, and H. Hu, [arXiv:2003.03246](https://arxiv.org/abs/2003.03246).
- [67] J. D. Jackson, *Classical Electrodynamics*, (3rd Edition ed. (Wiley & Sons, New York, 1999).
- [68] S. Coleman, in *Electromagnetism: Paths to Research*, 1st ed., edited by Doris Teplitz (Plenum, New York, 1982).
- [69] G. N. Watson, *Theory of Bessel Functions* (Cambridge University, Cambridge, England, 1922).